

Constraining GREA, an alternative theory accounting for the present cosmic acceleration

R. Calderon^{id, a} J. García-Bellido^{id, b} B. Vos-Ginés^{id, c}
 V. Gonzalez-Perez^{id, c} A. Shafieloo^{id, d,e} J. Aguilar^f S. Ahlen^{id, g}
 D. Bianchi^{id, h,i} D. Brooks^j T. Claybaugh^f A. de la Macorra^{id, k}
 J. E. Forero-Romero^{id, l,m} E. Gaztañaga^{id, n,o,p} S. Gontcho A
 Gontcho^{id, f,q} G. Gutierrez^r K. Honscheid^{id, s,t,u} C. Howlett^{id, v}
 M. Ishak^{id, w} R. Joyce^{id, x} R. Kehoe^y T. Kisner^{id, f} A. Kremin^{id, f}
 O. Lahav^j A. Lambert^f M. Landriau^{id, f} M. Manera^{id, z,aa}
 R. Miquel^{ab,aa} F. Prada^{id, ac} I. Pérez-Ràfols^{id, ad} E. Sanchez^{id, ae}
 D. Schlegel^f M. Schubnell^{af,ag} J. Silber^{id, f} D. Sprayberry^x
 G. Tarlé^{id, ag} B. A. Weaver^x H. Zou^{id, ah}

Affiliations are in Appendix D

E-mail: calderon@fzu.cz, juan.garcia.bellido@uam.es

Abstract. The origin of the Universe’s late-time accelerated expansion remains unknown. The General Relativistic Entropic Acceleration (GREA) theory offers a compelling alternative to Λ CDM, attributing cosmic acceleration to entropy growth associated with cosmic and black hole horizons, without invoking a cosmological constant. We test GREA against the latest DESI DR2 Baryon Acoustic Oscillations (BAO), multiple Type Ia supernova compilations (Union3, Pantheon+, DES-SN5YR), and cosmic microwave background (CMB) distance measurements. While GREA is not nested within Λ CDM, it achieves a comparable goodness-of-fit, highlighting its potential as a theoretically motivated framework that circumvents some of the fine-tuning issues of the standard Λ CDM cosmology. We find that the best-fit model features a transient phantom crossing at $z \lesssim 2$, with $w_a \equiv dw(a=1)/da \simeq -0.3$, in good agreement with observations. However, its present-day value $w_0 \equiv w(z=0)$ is tightly constrained to be $w_0 \simeq -1$. Upcoming low-redshift (i.e. $z < 1$) cosmological probes, from both background and perturbations, will offer promising avenues for further exploring the viability of the GREA theory.

Contents

1	Introduction	1
2	Theoretical background	3
3	Datasets	4
4	Methodology	5
5	Results and Discussions	6
5.1	Late-time probes	6
5.2	The role of the CMB	7
5.3	Further constraining GREAs	12
6	Conclusions	13
A	Parameter Constraints	16
B	Comparison with DESI DR1	16
C	CMB Compression and comparison with CamSpec PR4	17
D	Author Affiliations	19

1 Introduction

The cause of the Universe’s accelerated expansion remains unknown. For the past two decades, the standard cosmological model (Λ CDM) has explained it through a cosmological constant, Λ [1]. While this model has been in remarkable agreement with a broad range of observations [2–6], it faces serious theoretical challenges, such as the fine-tuning and coincidence problems [7, 8], and lacks a fundamental explanation for its two main components: dark energy and dark matter. In addition, growing observational tensions and anomalies [9–13]—including discrepancies in the inferred values of the Hubble constant [14–16] and the amplitude of matter fluctuations¹ [18–21]—have raised questions about the validity of Λ CDM. More recently, data from the Dark Energy Spectroscopic Instrument (DESI), combined with other cosmological probes, have added to this picture by hinting at $\sim 4\sigma$ deviations from a Λ CDM expansion history [22, 23]. If confirmed, these results could represent the first evidence for new physics beyond Λ CDM. While they are often interpreted as signs of a dynamical dark energy component [22, 24–29], alternative explanations have been proposed, including exotic neutrino masses [30, 31] or non-standard dark matter evolution [32], among others [33–38].

Common approaches for modeling dark energy often rely on arbitrary parametrizations of the equation of state parameter, $w(z) = P/\rho$, or non-parametric reconstruction techniques [39–44], which provide limited physical insight. Parametric models, such as w_0w_a CDM

¹Although the latest results from the KiDS legacy are fully compatible with the inferred values from the CMB [17].

[45, 46], are widely used due to their simplicity and connection with known physics [26, 46–48]. However, they risk biasing the inference if the true $w(z)$ deviates significantly from the assumed (parametric) form. Non-parametric methods offer greater flexibility, but require careful validation and can be difficult to interpret physically. A more informative strategy is to explore models grounded in theoretical principles. In this work, we investigate General Relativistic Entropic Acceleration (GREA) [49], a theory in which cosmic acceleration arises from the entropy growth associated with cosmological horizons [50]. GREA offers a novel, conceptually motivated alternative to Λ CDM and allows for direct connections between cosmology and fundamental physics. In the cosmological context, the GREA theory predicts that the present acceleration of the universe could arise from the growth of entropy associated with cosmic [49] and black hole horizons [51], without the need to introduce a cosmological constant, providing an alternative dynamics to that of Λ CDM. The GREA theory gives a covariant formalism for out of equilibrium dynamics in the context of general relativity. A consequence of GREA is the explicit breaking of the time reversal invariance when there is entropy production. This drives an entropic force that behaves effectively like bulk viscosity with a negative effective pressure [51].

Already before the recent evidence of significant deviations from the standard model of cosmology through state-of-the-art observations by DES-Y5 SNe [52] and DESI [22–24, 26, 27, 53], GREA was found to provide an equally good description of cosmological observations than Λ CDM [54]. Furthermore, GREA not only explains the coincidence problem, but can also help ease the Hubble tension by shifting the coasting point (when the universe transitioned from matter domination to acceleration) to higher redshifts and extending the period of acceleration [55]. In a recent paper [55], we performed a detailed calculation of the background and linear matter perturbations with the assumption that the entropy growth responsible for the accelerated expansion comes from the homogeneous cosmological horizon. We could show that, in this case, the dynamics can be described in terms of just one parameter, α , the ratio of the spatial curvature to the horizon distance. A given value of α defines a unique expansion history of the universe, with a dynamics that differs from Λ CDM and gives an explicit prediction for all background observables, like the values of the matter and dark energy content of the universe, the rate of expansion today, the coasting point, the value of the equation of state of dark energy and its derivative, the angular diameter and luminosity distances, etc. In this work, we use different observational datasets, including the latest baryon acoustic oscillation (BAO) measurements from DESI, to constrain the expansion history, as predicted by GREA.

This paper is structured as follows. In [Section 2](#), we introduce the theoretical background and details of GREA. We describe the observational datasets in [Section 3](#), and the methodology used in the analysis in [Section 4](#). Finally, we present our results in [Section 5](#) and conclude in [Section 6](#).

2 Theoretical background

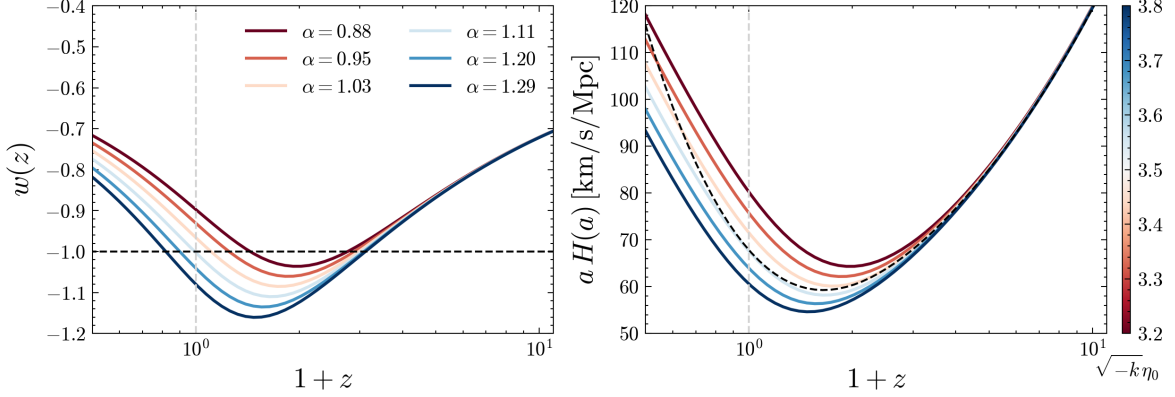


Figure 1. *Left:* The equation of state in GREA, for various values of the parameter α (or, equivalently $\sqrt{-k}\eta_0$), as obtained by integrating Eq. (2.1) with initial (CMB-asymptotic) $\Omega_m = 0.31, h = 0.678$. Note that for some parameter combinations, the *effective* w in GREA features a (transient) phantom crossing—without violating the NEC—and generically predicts a slope of $w_a \simeq -0.3$, in line with observations *Right:* $\dot{a} \equiv aH(a)$ as a function of redshift. The dashed black lines in both figures correspond to Λ CDM.

To obtain the expansion history of the Universe in GREA, we numerically solve for the (rescaled) conformal time $\tau \equiv H_0\eta = H_0 \int \frac{dt}{a(t)}$, using

$$\tau' \equiv \frac{d\tau}{da} = \left[a^2 \sqrt{\Omega_{m,0}a^{-3}(1 + \frac{a_{\text{eq}}}{a}) + \frac{4\pi}{3a^2} \frac{\sinh(2\tau)}{(-k)^{3/2}V_c}} \right]^{-1}, \quad (2.1)$$

where $a_{\text{eq}} \equiv \Omega_{r,0}/\Omega_{m,0}$ is the scale factor at matter-radiation equality, and where $\Omega_{r,0} = \Omega_{\gamma,0} + \Omega_{\nu,0}$ accounts for photons and (massless) neutrinos and $\Omega_{m,0} = \Omega_{b,0} + \Omega_{\text{cdm},0}$ for baryons and cold dark matter, respectively. In this framework, it is possible to show (see [55]) that the comoving volume, V_c , is related to the spatial curvature, k , and the conformal time $\eta_0 = \eta(z=0)$ by

$$(-k)^{3/2}V_c = \pi \left[\sinh(2\sqrt{-k}\eta_0) - 2\sqrt{-k}\eta_0 \right]. \quad (2.2)$$

It is the second term in Eq. (2.1) that plays the role of the dark energy, and drives the late-time accelerated expansion of the Universe. The phenomenology of GREA can be characterized with a single $\mathcal{O}(1)$ parameter, α , defined as [55]

$$\alpha \mathcal{D}_H(z=0) = \sqrt{-k}\eta_0, \quad (2.3)$$

where $\mathcal{D}_H(a) \equiv H(a)d_H(a) = Ha\eta(a)$ is the *dimensionless* horizon distance, computed from Eq. (2.1)². Its value today is $\mathcal{D}_H(z=0) \neq \eta_0$. As is clear from Eq. (2.3), α determines the size of the curvature scale, $\sqrt{-k}\eta_0$, relative to the causal horizon today. We integrate Eq. (2.1) with initial conditions deep in the radiation era $\tau(a_{\text{ini}} = 10^{-11}) = a_{\text{ini}}/\sqrt{\Omega_\gamma + \Omega_\nu}$, giving $\tau(a)$. The effect of varying α on the *effective* equation of state component, $w \equiv P/\rho$, and expansion history is shown in Fig. 1, where the corresponding values for $\sqrt{-k}\eta_0$ are reported in the color bar, and where the black dashed line depicts the Λ CDM predictions.

²In w CDM, this is given by $\mathcal{D}_H(a) = \frac{2}{\sqrt{\Omega_m}}a^{3/2} \cdot {}_2F_1\left[\frac{1}{2}, \frac{-1}{6w}, 1 - \frac{1}{6w}, \frac{\Omega_m - 1}{\Omega_m}a^{-3w}\right]$.

3 Datasets

To derive cosmological constraints on GREAs, we use the most recent Baryon Acoustic Oscillations (BAO) observations from the Dark Energy Spectroscopic Instrument (DESI) [24] along with different supernovae Ia (SNe Ia) compilations and cosmic microwave background (CMB) data. Here we briefly explain the data and methods we use in this analysis.

Our main observational data set is the baseline Baryon Acoustic Oscillations (BAO) data (DR2) from the Dark Energy Spectroscopic Instrument (DESI) [24, 26, 56]. We combine the DESI DR2 BAO data with complementary data sets: Supernovae Ia, Cosmic Microwave Background and Big-Bang Nucleosynthesis, as described below.

Baryon Acoustic Oscillations (BAO) This dataset, abbreviated as “DESI BAO”, spans seven redshift bins from $z = 0.3$ to $z = 2.33$ (where the last bin extends out to $z \approx 3.5$) [57]. DESI is an optical spectroscopic Stage IV survey carrying out a 3-D map over 14,000 square degrees and within the redshift range $0.1 < z < 4.2$ [58–65]. DESI was designed to improve cosmological constraints on both the expansion history and the growth rate of large scale structure, through measurements of the clustering of galaxies (BGS, LRGs and ELGs), quasars or QSOs, and the Lyman- α forest [66–69]. In this work, we use the BAO measurements from the first 3 years of DESI observations [70]. The galaxy and quasar BAO measurements used here are in configuration space [57].

Transverse to the line of sight, DESI constrains the ratio between the comoving angular diameter distance, D_M , at the effective redshift of the galaxy sample, z_{eff} , and the sound horizon at drag time, $r_d \equiv r_s(z_{\text{drag}})$, [57]:

$$\frac{D_M(z_{\text{eff}})}{r_d} \equiv \frac{c}{r_d} \int_0^{z_{\text{eff}}} \frac{dz'}{H(z')} = \frac{c}{H_0 r_d} \int_0^{z_{\text{eff}}} \frac{dz'}{E(z')} , \quad (3.1)$$

where c is the speed of light and $E(z) = H(z)/H_0$ is the normalized Hubble rate. The radial measurements of the BAO constrain the ratio between the Hubble distance $D_H \equiv c/H(z)$, at the effective redshift of the galaxy sample, z_{eff} , and the sound horizon at drag epoch, r_d :

$$\frac{D_H(z_{\text{eff}})}{r_d} \equiv \frac{c}{H(z_{\text{eff}})r_d} = \frac{c}{H_0 r_d} \frac{1}{E(z_{\text{eff}})} , \quad (3.2)$$

In the equations above, Eqs. (3.1) and (3.2), we explicitly factored out the absolute scaling set by the (degenerate) combination $H_0 r_d$. For the lowest redshift bin, corresponding to the BGS sample, we use the volume-averaged quantity:

$$\frac{D_V(z_{\text{eff}})}{r_d} \equiv [z_{\text{eff}} D_M^2(z_{\text{eff}}) D_H(z_{\text{eff}})]^{1/3} / r_d . \quad (3.3)$$

One crucial quantity for the analysis is the sound horizon, r_s , defined as

$$r_s(z) = \int_z^\infty \frac{c_s(z')}{H(z')} dz' , \quad (3.4)$$

where $c_s(z)$ is the sound speed of the photon-baryon plasma, given by

$$c_s^2(z) = \frac{c^2}{3(1 + \frac{3}{4}R(z))} , \quad R(z) \equiv \frac{\rho_b(z)}{\rho_\gamma(z)} , \quad (3.5)$$

and c denotes the speed of light in vacuum. The sound horizon in Eq. (3.4) is evaluated at the baryon drag epoch $z_{\text{drag}} \simeq 1066$, and at recombination $z_* \simeq 1089$. The exact values for z_{drag} and z_* are obtained using the approximations presented in [71]. These approximations provide subpercent accuracy for a wide range of parameter values, and they are further justified by the fact that at high-redshifts, GREA has a Λ CDM-like expansion history. This is shown in the right panel of Fig. 1.

Supernovae Ia (SNe Ia) We use supernova (SN) data from three sets: “Pantheon+”, “Union3”, and “DES-SN5YR”. “Pantheon+” is a compilation of 1550 supernovae spanning the redshift range $0.01 < z < 2.26$ [72]. “Union3” contains 2087 SNe Ia processed through the Unity 1.5 pipeline based on Bayesian Hierarchical Modelling [73]. “DES-SN5YR” is a compilation of 194 low-redshift SNe Ia ($0.025 < z < 0.1$) and 1635 photometrically classified SNe Ia covering the range $0.1 < z < 1.3$ [52]. These constrain the distance modulus

$$\mu(z) = m_B(z) - M_B = 5 \log_{10}(D_L(z)/\text{Mpc}) + 25 , \quad (3.6)$$

where $D_L(z) = (1+z)D_M(z)$ is the luminosity distance, encoding the cosmological model-dependence. $m_B(z)$ and M_B are the apparent and absolute magnitude, respectively. In this work, we treat M_B as a nuisance parameter.

SH0ES measurement of H_0 The Pantheon+ sample includes a set of very low-redshift Type Ia supernovae with Cepheid-based distance calibrations [14, 72]. These serve as the local anchor in the distance ladder and effectively constrain the Hubble constant, H_0 , or equivalently, the absolute magnitude of Type Ia supernovae, M_B . In practice, we use the `pantheonplusshoes`³ likelihood, as implemented in COBAYA⁴, and refer to this as Pantheon+ & SH₀ES .

Cosmic Microwave Background (CMB) Following [23, 74], we use the compressed CMB information in terms of $(\theta_s, \omega_b, \omega_{\text{cb}})$. These have been found to yield nearly identical constraints on late-time dark energy as the full CMB likelihood. The mean values and covariance matrix have been extracted from the publicly available⁵ P-ACT Λ CDM chains [75, 76], and include both Planck PR4 [77] and ACT DR6 lensing [78, 79]).

Big-Bang Nucleosynthesis (BBN) When we don’t include the CMB data, we include a prior on $\omega_b \equiv \Omega_b h^2$ from big-bang nucleosynthesis (BBN) [80] to break the H_0 - r_{d} degeneracy and “calibrate” the distances from BAO and SNe.

4 Methodology

To confront the predictions of GREA to the data, we numerically implement Eq. (2.1) into a Python package, `greapy`⁶. We then sample the posterior distribution of GREA using Markov Chain Monte Carlo (MCMC) methods. In particular, we use the Metropolis-Hastings algorithm [81, 82], as implemented in the publicly available sampler COBAYA [83]. The parameter space associated with GREA is $\Theta = \{H_0, \omega_{\text{cdm}}, \omega_b, \sqrt{-k}\eta_0\}$ and unless specified otherwise, we assume flat uninformative priors on all parameters, listed in Table 1. Throughout this

³https://cobaya.readthedocs.io/en/latest/likelihood_sn.html

⁴<https://github.com/CobayaSampler/cobaya>

⁵The chains can be found at <https://act.princeton.edu/act-dr6-data-products>

⁶<https://github.com/rcalderonb6/greapy>

Table 1. Parameters and priors used in the analysis. All of the priors are uniform in the ranges specified below, except for the runs including +BBN, where a Gaussian prior on ω_b is used instead [80].

parameter	prior
$\omega_{\text{cdm}} \equiv \Omega_{\text{cdm},0} h^2$	$\mathcal{U}[0.05, 0.5]$
$\omega_b \equiv \Omega_{b,0} h^2$	$\mathcal{U}[0.005, 0.1]$
$H_0 [\text{km s}^{-1} \text{Mpc}^{-1}]$	$\mathcal{U}[20, 100]$
$\sqrt{-k}\eta_0$	$\mathcal{U}[1, 5]$
$\Omega_{k,0}$	$\mathcal{U}[-0.3, 0.3]$

work, we assume massless neutrinos, with $N_{\text{eff}} = 3.044$ and a fixed spectral index, $n_s = 0.965$. We do not expect the inclusion of massive neutrinos or a different spectral tilt to significantly alter our conclusions, as none of the observables used in the analysis are sensitive to such parameters. We assess the convergence of our MCMC chains using the Gelman-Rubin ($R-1$) criterion [84] and require all of our chains to satisfy $R-1 < 0.01$. We analyze our chains and produce our plots using the python package `GetDist` [85]. Finally, for the Pantheon+, DES-SN5YR, and Union3 likelihoods, the marginalization over the absolute magnitude M_B is done analytically. As in previous DESI analyses, we adopt the α_{\perp} and α_{\parallel} parametrization to characterize the angular and radial BAO scales relative to a fiducial Λ CDM model. While a fully consistent treatment would involve recomputing the anisotropic two-point correlation function within the GREA framework, this is beyond the scope of the present work. Nonetheless, we note that the standard BAO compression scheme has been shown to be robust for a wide class of cosmological models, including those beyond Λ CDM [86]. In particular, GREA belongs to the class of homogeneous and isotropic FLRW models, and its linear perturbation theory yields a growth history (Fig. 9) that encompasses that of Λ CDM [55]. The primary difference lies in the dynamical evolution of the effective dark energy component.

To compute the Bayesian Evidence \mathcal{Z} required for model selection, we use the nested-sampling algorithm implemented in `POLYCHORD` [87, 88] for specific data combinations. In essence, Bayesian Evidence enables the direct comparison of competing models via their ratio, known as the Bayes factor, K , which quantifies the relative support for one model over another by simultaneously considering the goodness of fit and penalizing for model complexity. However, it is important to note that model selection based on the Bayes factor has limitations, and conclusions drawn from such analyses must be interpreted with caution [89–91]. The interpretation of the Bayes factor can be sensitive to the choice of priors, not only parameter ranges but also theoretical priors, and its effectiveness may diminish when comparing models that differ significantly in their underlying theoretical assumptions or parameter space.

5 Results and Discussions

5.1 Late-time probes

We begin by discussing the results obtained from late-time (low-redshift) probes. Fig. 2 presents the constraints derived from combining the DESI DR2 BAO measurements with various available supernova Ia (SNe Ia) compilations (Section 3). The light gray (unfilled) contours represent the uncalibrated DESI BAO and Pantheon+ datasets, which constrain only the fractional matter density, $\Omega_{m,0}$, and the absolute scaling, $H_0 r_d$. The uncalibrated

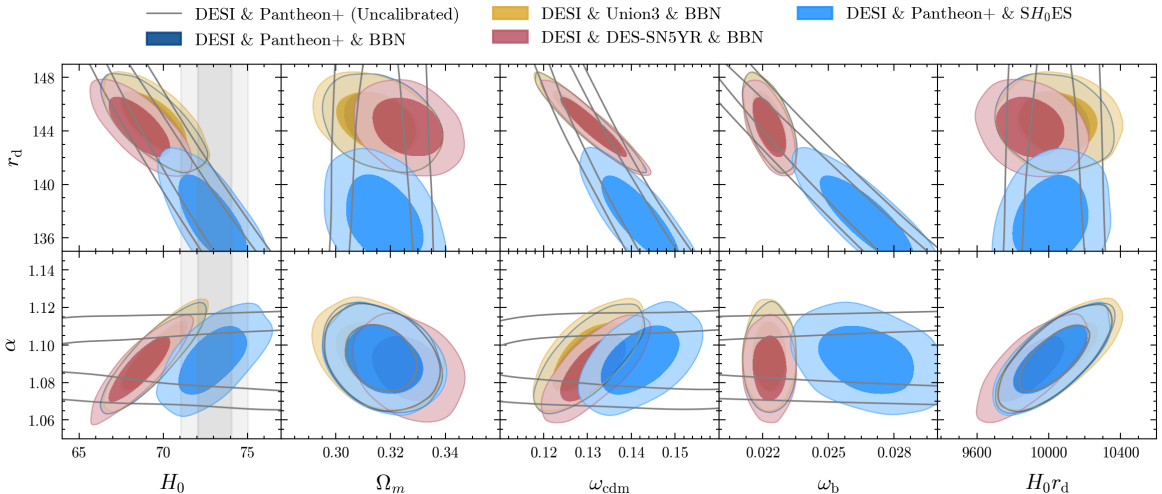


Figure 2. Marginalized constraints on parameters of GREA from DESI BAO DR2 and the various SNe Ia compilations: “Pantheon+”, “Union3”, and “DES-SN5YR” (Section 3). We show the impact of an early-universe calibration of distances through the inclusion of a BBN-prior on $\omega_b \equiv \Omega_b h^2$ [80], or at late-times by including SH0ES [14]. The light gray unfilled contours show the uncalibrated results when using the DESI BAO and Pantheon+ datasets, which constrain only the product $H_0 r_d$ and $\Omega_{m,0}$. For reference, we show here the H_0 measurements from SH0ES [14] with the light grey vertical bands. The inferred parameters are consistent for the Pantheon+, Union3, and DES-SN5YR SN datasets.

distances probed by the SN+BAO combination constitute a sensitive probe of the shape of the expansion history $E(z) \equiv H(z)/H_0$, as seen from Eqs. (3.1), (3.2) and (3.6). Thus, the *uncalibrated* SN+BAO data alone can constrain the fractional matter density, $\Omega_{m,0}$, and α , but not the individual physical densities ω_b and ω_c .

The late-time probes (SN & BAO) allow for values of H_0 compatible with SH0ES [14] (shown as a vertical shaded band in Fig. 2) while implying a reduced size of the sound horizon, relative to Λ CDM, and therefore an increase in ω_b (in tension with BBN). Such a value of H_0 , in combination with a large $\Omega_{m,0}$, inevitably leads to an increase of $\omega_m = \omega_{\text{cdm}} + \omega_b = \Omega_{m,0} h^2$ (Fig. 2). This is common to many models attempting to address the Hubble tension, as recently emphasized in [92, 93]. Such an increase in the physical matter density has important implications for the acoustic peaks in the cosmic microwave background and the clustering of matter at late times.

To break the H_0 - r_d degeneracy, we also incorporate a big-bang nucleosynthesis (BBN) prior on $\omega_b = (2.231 \pm 0.05) \times 10^{-2}$ [80], effectively calibrating distances in the early universe by fixing the size of the standard ruler, r_d . The constraints on $\alpha = 1.09 \pm 0.012$ are stable across different SN compilations, while the constraints on $\Omega_{m,0}$ marginally depend on the choice of SN, with DES-SN5YR driving the preference for higher matter densities with respect to Pantheon+ and Union3, in agreement with previous findings [24, 26, 52, 56]. For conciseness, in what follows we will focus on and only show results using the Pantheon+ compilation.

5.2 The role of the CMB

In Fig. 3, we report the constraints including CMB information. The CMB constrains the late-time expansion history primarily through an exquisite ($\sim 0.04\%$) measurement of the acoustic scale $\theta_s \equiv r_s(z_*)/D_M(z_*)$. Recall that the relative height of odd/even acoustic

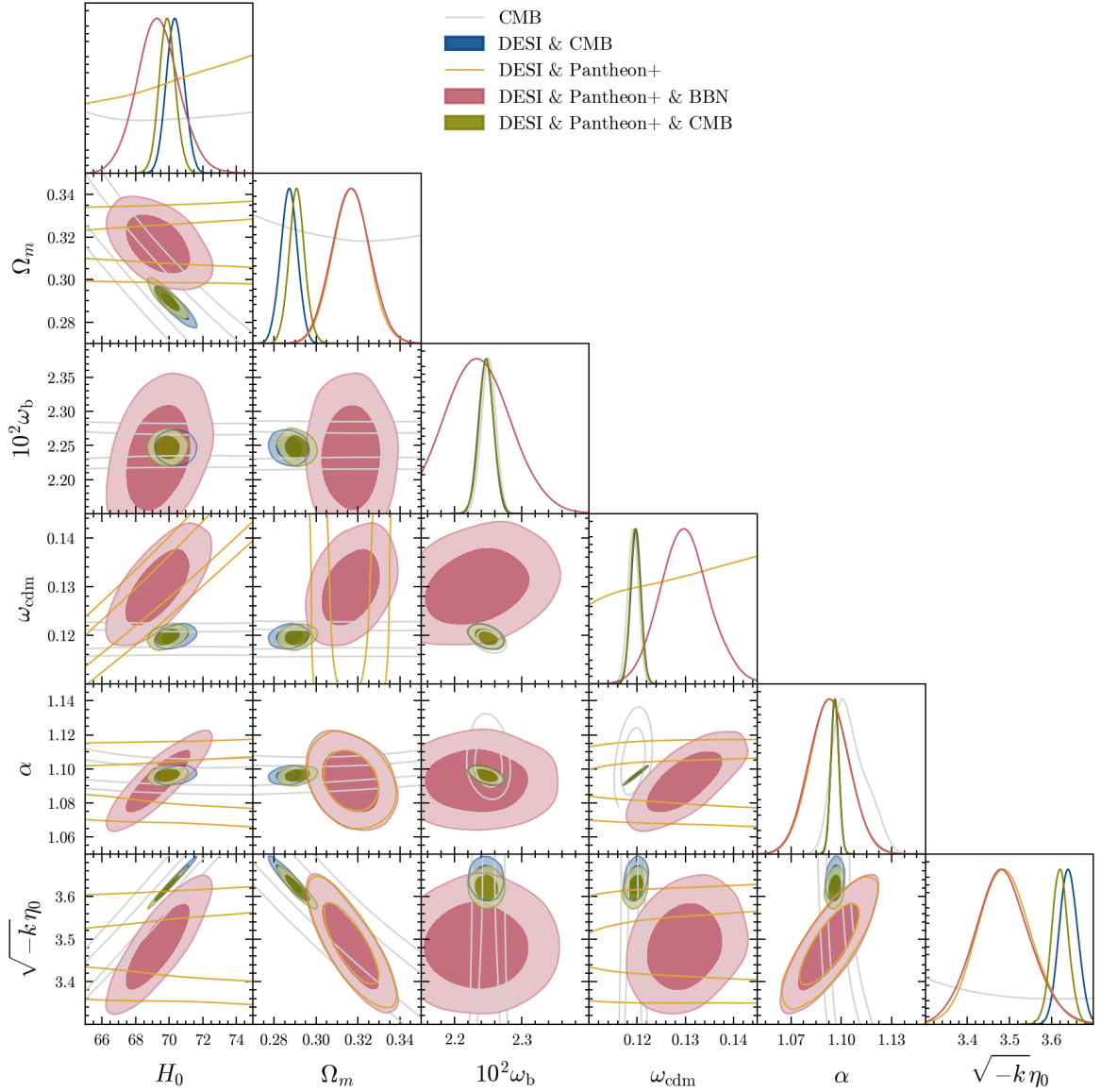


Figure 3. The full posterior distribution for GREA’s cosmological parameters (Section 2), inferred from fitting the model to different datasets, including DESI DR2 [74], as indicated in the legend. The light gray unfilled contours show the uncalibrated results when using the CMB data from P-ACT (Section 3), which is sensitive to the product $\Omega_{m,0}h^2$. Note that the Pantheon+ data prefer higher matter densities than the DESI & CMB datasets, leading to some tension in some of the projected parameter space. These inconsistencies are also reflected in the degraded fit to the data.

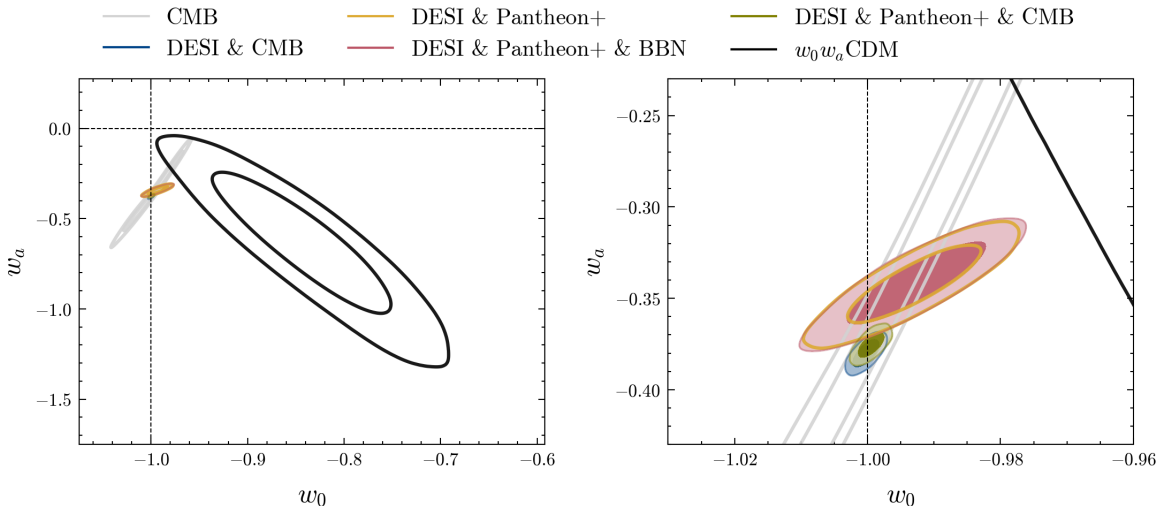


Figure 4. *Left:* Derived constraints on the equation of state parameter $w(a = 1)$ and its derivative $w_a = -\frac{dw}{da}(a = 1)$ today for GREA. Note that the parametrization $w(a) = w_0 + w_a(1 - a)$ does not capture the full behavior of the equation of state in GREA (Fig. 1). These two parameters only capture the very low- z behavior, and we report them here for comparison with the standard w_0 - w_a analysis. A negative slope $w_a \sim -0.3$ is quite a generic prediction from GREA, while its value today w_0 , depends on the value of α , as illustrated in Fig. 1. *Right:* Zoomed in version around the region favoured by GREA.

peaks in the CMB tightly constrains the physical baryon density, $\omega_b = \Omega_{b,0}h^2$ [94, 95]. Thus, the angular size of the sound horizon, together with the physical energy densities ω_b and ω_{cdm} , carries most of the geometrical information contained in the CMB. Within ΛCDM , the CMB distance priors provide constraints on the fractional matter density, $\Omega_{m,0}$, and Hubble constant, H_0 . In GREA, however, because of the degeneracies introduced by the parameter α , we can no longer estimate $\Omega_{m,0}$ and H_0 purely from such measurements (as shown by the gray contours in Fig. 3). This is reminiscent of the intrinsic geometrical degeneracy between matter and dark energy ($\Omega_{m,0}$ and $w(z)$) [e.g. 43, 96–99].

Let us now discuss the results of the DESI BAO & CMB combination. While the CMB is sensitive to the product $\Omega_{m,0}h^2$, DESI BAO measurements probe the fractional matter density $\Omega_{m,0}$ directly. Thus, including the DESI data breaks these degeneracies by providing constraints on $\Omega_{m,0}$ (see Figure 4). In turn, this allows for an estimation of H_0 , and more importantly, of α , which characterizes the phenomenology of GREA. Including SNe Ia distance measurements, which are also highly sensitive to the fractional matter density, yield constraints of $\Omega_{m,0} = 0.317 \pm 0.009$ ($\Omega_{m,0} = 0.292 \pm 0.004$) for the DESI BAO & Pantheon+ & BBN (DESI BAO & Pantheon+ & CMB) combination. This increase in $\Omega_{m,0}$ ultimately leads to a lower estimate of α , shifting the central value of H_0 towards smaller values, around $H_0 \sim 70$ for any analysis including both Pantheon+ and DESI BAO data. Notably, swapping Pantheon+ with the DES-SN5YR compilation pushes H_0 to even lower values, due to the preference for a higher $\Omega_{m,0}$ in comparison to Pantheon+.

These differences in $\Omega_{m,0}$ between analyses with and without Pantheon+ are reflected in the degraded fit quality to the combined data, as shown in Table 2. This fit degradation, driven by subtle differences in preferred $\Omega_{m,0}$, is a key reason why many late-time modifications to the expansion history struggle to resolve the “cosmic calibration” problem

Table 2. The goodness of fit for different models and dataset combinations, $\Delta\chi^2$, obtained with the minimizer iMINUIT [101]. The second column shows $\Delta\chi^2 \equiv \chi^2_{\text{GREA}} - \chi^2_{\Lambda\text{CDM}}$. Note that CMB here refers to Planck PR4.

Data	$\Delta\chi^2$	χ^2_{GREA}	$\chi^2_{\Lambda\text{CDM}}$	$\chi^2_{\Lambda\text{CDM}+\Omega_k}$	$\chi^2_{w_0w_a}$
DESI & BBN	3.6	13.9	10.3	9.9	5.6
DESI & CMB	3.0	17.0	13.9	10.5	7.3
DESI & Pantheon+ & BBN	5.9	1422.1	1416.2	1414.4	1411.3
DESI & Pantheon+ & PR4	13.4	1433.5	1420.1	1416.0	1413.0
DESI & Pantheon+ & SH ₀ ES	5.8	1471.2	1465.3	1463.6	1460.5
DESI & Pantheon+ & PR4 & SH ₀ ES	0.4	1498.2	1497.8	1490.1	1490.4

[16, 92, 100], especially when combining the Hubble diagrams probed by SNe Ia and BAO.

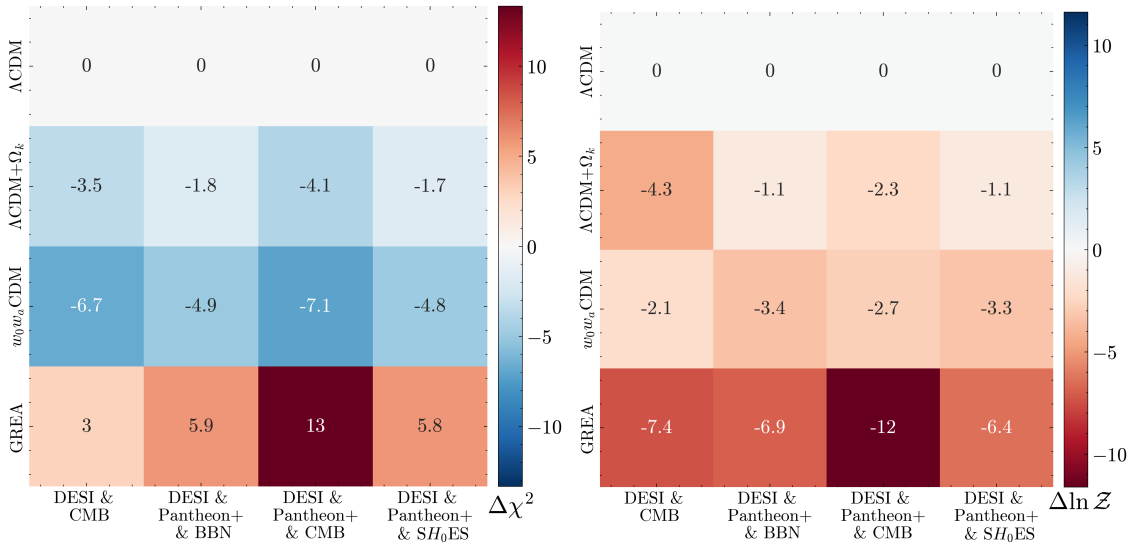


Figure 5. Visual representation of the goodness of fit compared to the ΛCDM model, for the different models and dataset combinations as shown in Table 2: $\Delta\chi^2 \equiv \chi^2_i - \chi^2_{\Lambda\text{CDM}}$ (left), and $\Delta\ln\mathcal{Z} = \log\mathcal{Z}^i - \log\mathcal{Z}^{\Lambda\text{CDM}}$ values (right). The Bayesian evidence, \mathcal{Z} , is computed using POLYCHORD [88].

Finally, it is insightful to introduce an *effective* dark energy density $\rho_{\text{DE}}^{\text{eff}}$ as

$$\Omega_{\text{DE},0} f_{\text{DE}}(z) \equiv \left(\frac{H(z)}{H(0)} \right)^2 - \Omega_{\text{m},0}(1+z)^3 - \Omega_{\text{r},0}(1+z)^4, \quad (5.1)$$

where $\Omega_{\text{DE},0} = \frac{8\pi G}{3H(0)^2} \rho_{\text{DE},0}^{\text{eff}} \simeq (1 - \Omega_{\text{m},0})$ and $f_{\text{DE}}(z) = \rho_{\text{DE}}^{\text{eff}}(z)/\rho_{\text{DE},0}^{\text{eff}}$ determines its redshift evolution, from which we can compute its *effective* equation of state, using

$$w(a) = -\frac{1}{3} \frac{d\ln f_{\text{DE}}}{d\ln a} - 1 = -\frac{1}{3} \frac{d\ln}{d\ln a} \left[\frac{\sinh(2\tau)}{a^2} \right] - 1 \quad (5.2)$$

$$= -\frac{1}{3} \left[2a \tau'(a) \coth[2\tau(a)] + 1 \right]. \quad (5.3)$$

The marginalized constraints on these two key quantities are depicted in Fig. 6 for the DESI & Pantheon+ & CMB data combination. These two quantities allow for a direct

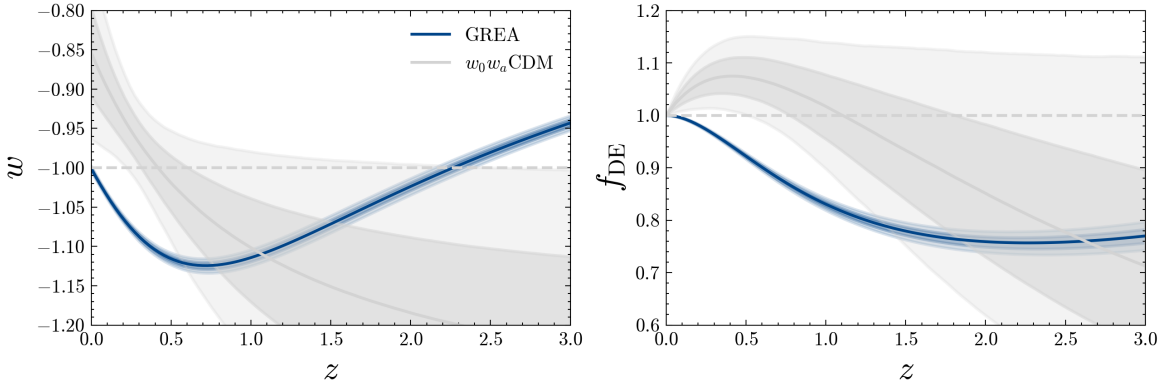


Figure 6. Constraints on the equation of state, w , and normalized energy density, $f_{\text{DE}} = \rho_{\text{DE}}/\rho_{\text{DE},0}$, from the DESI & Pantheon+ & CMB data combination in w_0w_a CDM (in gray) and GREA (in blue). The shaded bands represent the 68% and 95% confidence levels computed by drawing a large number of samples from the chains.

comparison of the best-fit GREA model with the data-driven (model-agnostic) reconstructions of the DE phenomenology, presented in [24, 28, 29]. The behaviour of $w(z)$ in GREA, particularly at low redshift, does not fully match the trends suggested by non-parametric, model-independent reconstructions. This mismatch is also reflected in the fit to the data, where the phenomenological w_0w_a CDM model—whose functional form closely follows the reconstructed $w(z)$ —consistently outperforms both Λ CDM and GREA. While this discrepancy could have been anticipated from the allowed shape of $w(z)$ in GREA (Fig. 1) even before fitting, it is still valuable to confront the model with data, as this allows us to constrain its parameters and quantitatively assess its viability.

In Fig. 7, we display the best-fit predictions for the different models on top of BAO observables $D_V(z)/r_d$ and $F_{\text{AP}}(z) \equiv D_M/D_H$ normalized to their fiducial values⁷. The isotropic and anisotropic BAO distortion parameters at $0 < z < 1$ can help distinguish the best fit GREA and the w_0w_a CDM models (see Fig. 7).

When fitting the combined (DESI & Pantheon+ & CMB) data, the high-redshift evolution of the distance modulus is the same for both the best-fit GREA and w_0w_a CDM models describing current observations, except for very low redshift $z < 0.5$, where the increase in $H^{\text{GREA}} > H^{\Lambda\text{CDM}}$ leads to $D_L^{\text{GREA}} < D_L^{\Lambda\text{CDM}}$ (Fig. 8). Note that the uncalibrated Pantheon+ data (black circled datapoints) does not constrain H_0 , nor M_B , but only their product. Thus, for a given H_0 there is freedom to choose the corresponding M_B that best fits the data. For simplicity, we normalize these measurements to the fiducial Λ CDM value. When calibrating distances with the cepheids-based (SH₀ES) measurements (dashed lines in Fig. 8), as expected, the very low- z evolution is almost identical between the three models, and deviations only appear at intermediate redshift, where the w_0w_a CDM seems to fit the SN data better.

⁷This corresponds to the baseline Λ CDM parameters used by the AbacusSummit suite of N-body simulations https://github.com/abacusorg/AbacusSummit/blob/main/Cosmologies/abacus_cosm000/CLASS.ini. For more details on the BAO measurements, see e.g. [102].

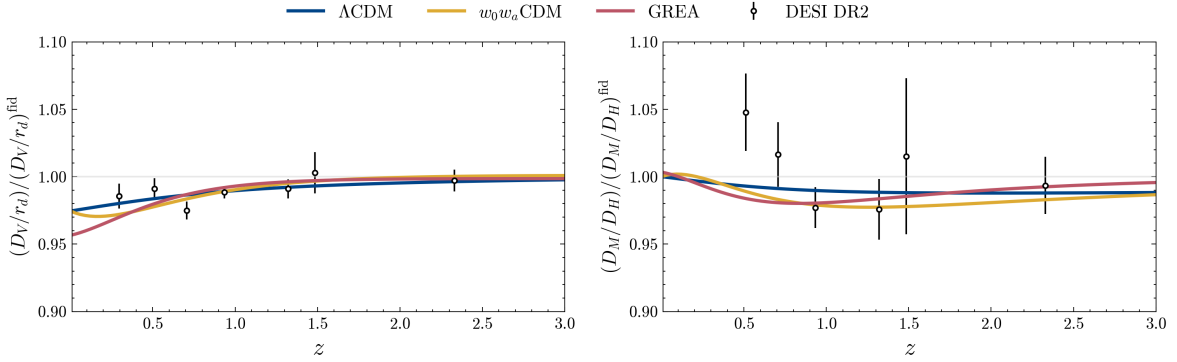


Figure 7. Evolution with redshift of the volume-averaged distance, D_V (left panel); and the anisotropic distortion measured with the comoving angular diameter distance signal, D_M (right panel, see details in Section 3). Observational datasets are shown as open symbols. In each panel, the best fit model (BAO & SNeIa & CMB) for Λ CDM is shown by blue lines, GREA by red lines, and the w_0w_a CDM model by yellow lines. The largest differences between the GREA and w_0w_a CDM best fit models are found at $z < 1$.

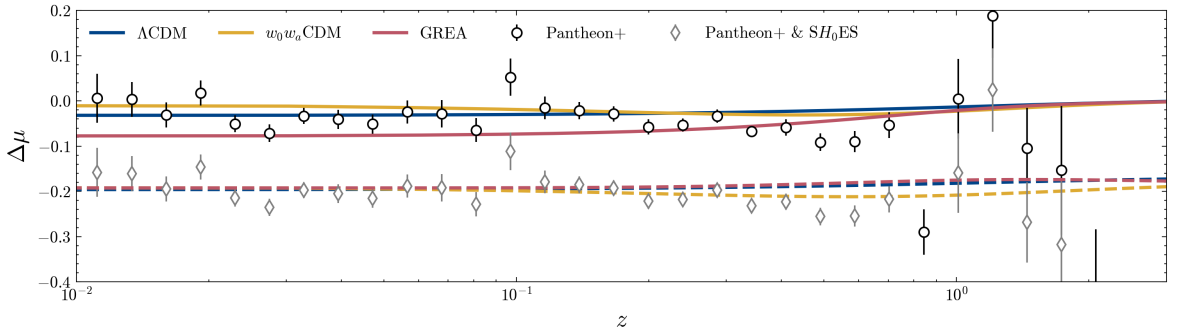


Figure 8. Evolution with redshift of the distance modulus residuals, $\Delta\mu = \mu - \mu^{\text{fid}}$. The (uncalibrated) Pantheon+ are shown as open symbols, whereas the SH₀ES -calibrated Pantheon+ measurements are shown as diamonds. The solid lines correspond to the best fit models to the full (DESI & Pantheon+ & CMB) data combination. The dashed lines shows the corresponding bestfit predictions to the SH₀ES -calibrated (DESI & Pantheon+) measurements.

5.3 Further constraining GREA

In GREA, for scales of cosmological interest, the growth of density perturbations (in the linear regime) obeys [55]

$$a(\tau)\delta''(\tau) + a'(\tau)\delta'(\tau) = \frac{3}{2}\Omega_{\text{m},0}\delta(\tau), \quad (5.4)$$

where $\delta = \rho/\bar{\rho} - 1$ is matter density contrast and a prime denotes differentiation with respect to conformal time, τ . The modified growth of perturbations stems from the modified evolution of the scale factor, $a(\tau) \neq a^{\Lambda\text{CDM}}$, encoded in the Hubble friction term above. It is convenient to rewrite the growth equation Eq. (5.4) in terms of the growth factor $f \equiv \delta'/\delta = \frac{d\ln\delta}{d\ln a}$, giving

$$f'(a) + \left(f(a) + 2 + \frac{E'}{E} \right) f(a) = \frac{3}{2}\Omega_{\text{m}}(a), \quad (5.5)$$

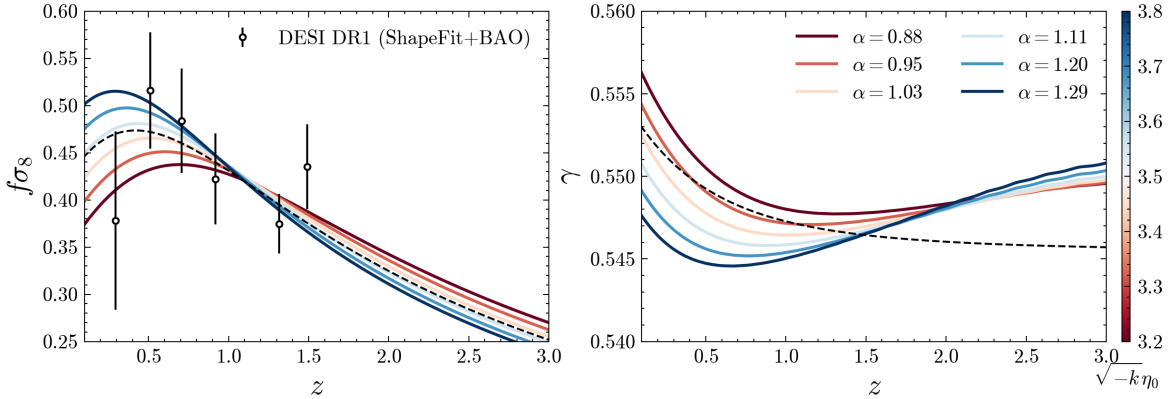


Figure 9. Growth of density perturbations as a function of redshift for various values of α in GREA. *Left:* Evolution of the combination $f\sigma_8(z)$, probed by redshift-space distortions. *Right:* Corresponding growth index $\gamma(z) \equiv \ln f(z) / \ln \Omega_m(z)$ evolution. The $f\sigma_8(z)$ measurements have been extracted from the DESI DR1 ShapeFit+BAO analysis [53]. They are for illustrative purposes only and have not been used in the present analysis. The black dashed line on both panels corresponds to Λ CDM.

where $' \equiv d/d \ln a$, $\Omega_m(a) = \Omega_{m,0} a^{-3} E^{-2}$ and $E = H(z)/H_0$. We integrate Eq. (5.5) with initial conditions deep in the matter dominated epoch, with $f(a_{\text{ini}}) = 1$ ⁸. From an observational viewpoint, the relevant quantity is the combination [103]

$$f\sigma_8(a) \equiv f(a) \cdot \sigma_8(a) = \frac{\sigma_{8,0}}{\delta_0} f\delta = \frac{\sigma_{8,0}}{\delta_0} \delta', \quad (5.6)$$

where $\sigma_{8,0}$ is the amplitude of matter fluctuations, smoothed over scales of radius $R = 8h^{-1}\text{Mpc}$, and $\delta_0 = \delta(z = 0)$. On the left panel of Fig. 9, we show the evolution of the growth rate $f\sigma_8(a)$ at late times for various GREA scenarios, along with the DESI DR1 measurements extracted from a ShapeFit+BAO analysis (Tab. 11 in [53]). The present data constrain the background expansion history in GREA to be close to that of Λ CDM, with preferred values of $\alpha \sim 1.09$, seen in Fig. 3 and Table 3. Therefore, the corresponding $f\sigma_8$ closely follows that of Λ CDM, as the growth history is fully determined by the expansion history for DE models inside GR. On the right panel, we display the evolution of the growth index $\gamma(z) \equiv \ln f(a) / \ln \Omega_m(a)$ [104–108]. Interestingly, while the present value of $\gamma \simeq 0.55$ is close to that of Λ CDM, at higher redshifts, $\gamma(z)$ has a very different behaviour, satisfying in particular $d\gamma/dz > 0$. This is in sharp contrast with the Λ CDM case, where $\gamma(z)$ is a monotonically decreasing function of redshift [109–111]. Forthcoming LSS measurements by DESI, in combination with Euclid and LSST, are expected to constrain γ and its derivative with high precision [112].

6 Conclusions

General Relativistic Entropic Acceleration (GREA) arises as a consequence of out of equilibrium phenomena associated with the growth of entropy of horizons. It is a consequence of quantum gravity holography, which gives a correspondence between the dynamics in a volume of space and the degrees of freedom in the boundary of that space. The GREA theory

⁸In an Einstein-DeSitter (EdS), or matter dominated universe, it is easy to show that $\delta(a) \propto a \Leftrightarrow f = 1$.

offers a natural explanation for the universe’s accelerated expansion without the need for a cosmological constant [49, 51, 54, 55]. The accelerated expansion in GREAs is associated with the growth of entropy from cosmic and black hole horizons, making it a promising alternative to the cosmological constant, Λ . In addition, this theory introduces a single $\mathcal{O}(1)$ parameter α that encapsulates the effect of GREAs as an evolving dark energy scenario, both at the background and perturbation level. GREAs makes precise predictions for various cosmological observables that can be tested with increasingly accurate observations [55]. For our Universe, the causal horizon growth associated with the matter/energy content induces a growth in entropy of the horizon while driving a dynamical entropic acceleration, which is very different from that predicted by Λ CDM. Even in the absence of Λ , the entropic acceleration is enough to explain the dimming of distant SNe and the recent BAO data from DESI DR2 (Fig. 7). Moreover, GREAs makes a specific prediction: that the size of our causal horizon today should be the same as the curvature scale ($\alpha \sim 1$).

In this work, we have used state-of-the-art BAO measurements by the DESI collaboration [56, 57, 60, 69, 102], together with other external datasets (Section 3), to constrain the free parameters of GREAs (Section 4). GREAs achieves a fit to observations comparable to the phenomenological Λ CDM model⁹ (Table 2 and Fig. 5). This is particularly encouraging as Λ CDM and GREAs are not nested models. Despite the Bayesian evidence favouring the phenomenological Λ CDM model, the alternative GREAs scenario remains compelling. We emphasize that usual model comparison metrics, such as $\Delta\chi^2$ and the Bayes ratio, should be interpreted with care for non-nested models, such as GREAs and Λ CDM. We have reported the Bayes ratios assuming equal priors for the underlying models. Perhaps a more appropriate choice is to weight the alternative hypothesis according to their theoretical basis. This could potentially penalize Λ CDM and w_0w_a CDM with respect to GREAs and change the odds in its favour. In the Bayesian framework, the preference for one model (M_1) over another (M_0) is usually assessed by computing the Bayes ratio, K , given by

$$K = \frac{\mathcal{Z}_1}{\mathcal{Z}_0} = \frac{\mathcal{P}(D|M_1)}{\mathcal{P}(D|M_0)} = \frac{\mathcal{P}(M_1|D)\Pi(M_0)}{\mathcal{P}(M_0|D)\Pi(M_1)}, \quad (6.1)$$

where $\Pi(M_i)$ and $\mathcal{Z}_i = \mathcal{P}(D|M_i)$ are the prior probability and evidence for model M_i , respectively. The quantity $\mathcal{P}(M_i|D)$ is precisely what we want to estimate; that is, the probability of the model, given the observed data. Most of the times, we assume $\Pi(M_1) = \Pi(M_0) = 0.5$, as most DE models are purely phenomenological, and we cannot favour one over the other, purely on theoretical grounds. The ratio of Bayesian evidences should be weighted according to the reliability of the model priors. In particular, having values of Λ orders of magnitude below quantum gravity expectations should heavily penalize Λ CDM when compared against GREAs. However, we have not taken this into account in our analysis and conclusions. We leave this analysis for a future publication.

Our analysis suggests that GREAs can account for the data to some extent without invoking a fine-tuned (infinitesimally small and positive) cosmological constant. The best GREAs model that fits the observational data point towards a *transient* phantom crossing at $z \leq 2$ (see Fig. 6). We note that we have worked under the assumption of a Λ CDM-expansion history at early times (in particular, at matter-radiation equality). It would be interesting to explore how alternative initial conditions, e.g., with an Early Dark Energy (EDE)-like component or modified physics at recombination, can alter the derived constraints. Moreover,

⁹We note that χ^2 differences are reported relative to Λ CDM. The goodness of fit of Λ CDM has been assessed in previous works [53, 70].

we have assumed that the main effect of GREA comes from the *homogeneous* entropy growth of the cosmic horizon. If GREA arises also from the gravitational collapse of *inhomogeneous* structures that form the cosmic web [51], it may modify the late universe dynamics in a way that could be tested with future cosmological data. This analysis, however, requires non-linear N-body simulations which go beyond the state-of-the-art. We leave this for future work.

Additional observational data will be critical to further assess the viability of GREA. Data at $z < 1$, probing the growth of cosmic structures and the evolution of matter perturbations will be particularly interesting (Fig. 9). Forthcoming measurements from DESI and other stage-IV experiments will provide an opportunity to rigorously test the predictions of GREA across a wider range of cosmological observables.

Acknowledgments

R.C. would like to thank Vivian Poulin and Tristan L. Smith for insightful discussions. This work was supported by the high-performance computing cluster Seondeok at the Korea Astronomy and Space Science Institute. R.C. is funded by the Czech Ministry of Education, Youth and Sports (MEYS) and European Structural and Investment Funds (ESIF) under project number CZ.02.01.01/00/22_008/0004632. J.G-B acknowledges support from the Research Project PID2021-123012NB-C43 [MICINN-FEDER], and the Centro de Excelencia Severo Ochoa Program CEX2020-001007-S at Instituto de Física Teórica. B.V.G would like to acknowledge the support from the European Union (ERC StG, LSS BeyondAverage, 101075919) and the Comunidad de Madrid 2019-T1/TIC-12702 grant. V.G.P. acknowledges support from Comunidad de Madrid in Spain (Atracción de Talento Contract grants: 2019-T1/TIC-12702 and 2023-5A/TIC-28943) and the Ministerio de Ciencia e Innovación (MICINN, grant PID2021-122603NB-C21). This material is based upon work supported by the U.S. Department of Energy (DOE), Office of Science, Office of High-Energy Physics, under Contract No. DE-AC02-05CH11231, and by the National Energy Research Scientific Computing Center, a DOE Office of Science User Facility under the same contract. Additional support for DESI was provided by the U.S. National Science Foundation (NSF), Division of Astronomical Sciences under Contract No. AST-0950945 to the NSF's National Optical-Infrared Astronomy Research Laboratory; the Science and Technology Facilities Council of the United Kingdom; the Gordon and Betty Moore Foundation; the Heising-Simons Foundation; the French Alternative Energies and Atomic Energy Commission (CEA); the National Council of Humanities, Science and Technology of Mexico (CONAHCYT); the Ministry of Science, Innovation and Universities of Spain (MICIU/AEI/10.13039/501100011033), and by the DESI Member Institutions: <https://www.desi.lbl.gov/collaborating-institutions>. Any opinions, findings, and conclusions or recommendations expressed in this material are those of the author(s) and do not necessarily reflect the views of the U. S. National Science Foundation, the U. S. Department of Energy, or any of the listed funding agencies.

The authors are honored to be permitted to conduct scientific research on I'oligam Du'ag (Kitt Peak), a mountain with particular significance to the Tohono O'odham Nation.

Data Availability

Data from the plots in this paper will be made available on Zenodo (<https://zenodo.org/records/XXXXXX>) as part of DESI's Data Management Plan.

Table 3. 68% credible intervals for the cosmological parameters in GREA, using various dataset combinations. We also report the *maximum a posteriori* (MAP) values in parentheses, obtained with the minimizer `iMINUIT` [101].

Datasets	$\Omega_{\text{m},0}$	$10^2 \omega_b$	$H_0 [\text{km s}^{-1} \text{Mpc}^{-1}]$	α
DESI & Pantheon+ (Uncalibrated)	0.323 ± 0.012 (0.316)	— (—)	— (—)	$1.1067^{+0.0044}_{-0.0049}$ (1.092)
DESI & BBN	0.300 ± 0.011 (0.298)	2.23 ± 0.05 (2.23)	70.9 ± 1.5 (70.8)	1.105 ± 0.013 (1.104)
DESI & Union3 & BBN	0.315 ± 0.010 (0.315)	2.23 ± 0.05 (2.23)	69.5 ± 1.3 (69.4)	1.094 ± 0.012 (1.092)
DESI & DES-SN5YR & BBN	0.326 ± 0.008 (0.325)	2.23 ± 0.05 (2.23)	68.6 ± 1.2 (69.5)	1.088 ± 0.012 (1.087)
DESI & Pantheon+ & BBN	0.317 ± 0.009 (0.316)	2.23 ± 0.05 (2.23)	69.4 ± 1.3 (69.4)	1.093 ± 0.012 (1.093)
DESI & PR4	0.288 ± 0.004 (0.287)	2.217 ± 0.014 (2.215)	70.4 ± 0.5 (70.4)	1.0994 ± 0.0029 (1.099)
DESI & P-ACT	0.287 ± 0.004 (0.287)	2.247 ± 0.011 (2.247)	70.4 ± 0.5 (70.4)	1.0962 ± 0.0023 (1.096)
DESI & Pantheon+ & PR4	0.292 ± 0.004 (0.292)	2.216 ± 0.014 (2.215)	69.9 ± 0.5 (69.9)	1.0995 ± 0.0027 (1.099)
DESI & Pantheon+ & P-ACT	0.291 ± 0.004 (0.291)	2.247 ± 0.011 (2.246)	69.9 ± 0.5 (69.8)	1.0961 ± 0.0024 (1.096)
DESI & Pantheon+ & SH ₀ ES	0.317 ± 0.009 (0.316)	2.68 ± 0.14 (2.646)	72.9 ± 1.3 (72.8)	1.092 ± 0.012 (1.093)
DESI & Pantheon+ & PR4 & SH ₀ ES	0.287 ± 0.004 (0.287)	2.218 ± 0.014 (2.218)	70.6 ± 0.5 (70.6)	1.0997 ± 0.0029 (1.100)
DESI & Pantheon+ & P-ACT & SH ₀ ES	0.286 ± 0.004 (0.285)	2.248 ± 0.011 (2.247)	70.5 ± 0.5 (70.6)	1.0967 ± 0.0024 (1.096)

A Parameter Constraints

In [Table 3](#), we report the marginalized constraints on the cosmological parameters of GREA, for the various data combinations considered in this work.

B Comparison with DESI DR1

Throughout this work, we have used the BAO constraints from DESI DR2. We explore how the constraints have improved going from DR1 to DR2 in [Fig. 10](#). DESI DR2 contains 6671 dark tiles, increasing by a factor of 2.4 the number of objects released in DR1[74].

We find that the constraints improved by a factor of ~ 2 when moving from DR1 to DR2. The central values stay within 1σ . The trends seen for the central values are similar to the results shown in [Fig. 2](#) when removing the SN data from the DESI DR2 & Pantheon+ & CMB. In terms of the curvature scale parameter, $\sqrt{-k}\eta_0$, the constraints in DR2 are 60% tighter than in DR1.

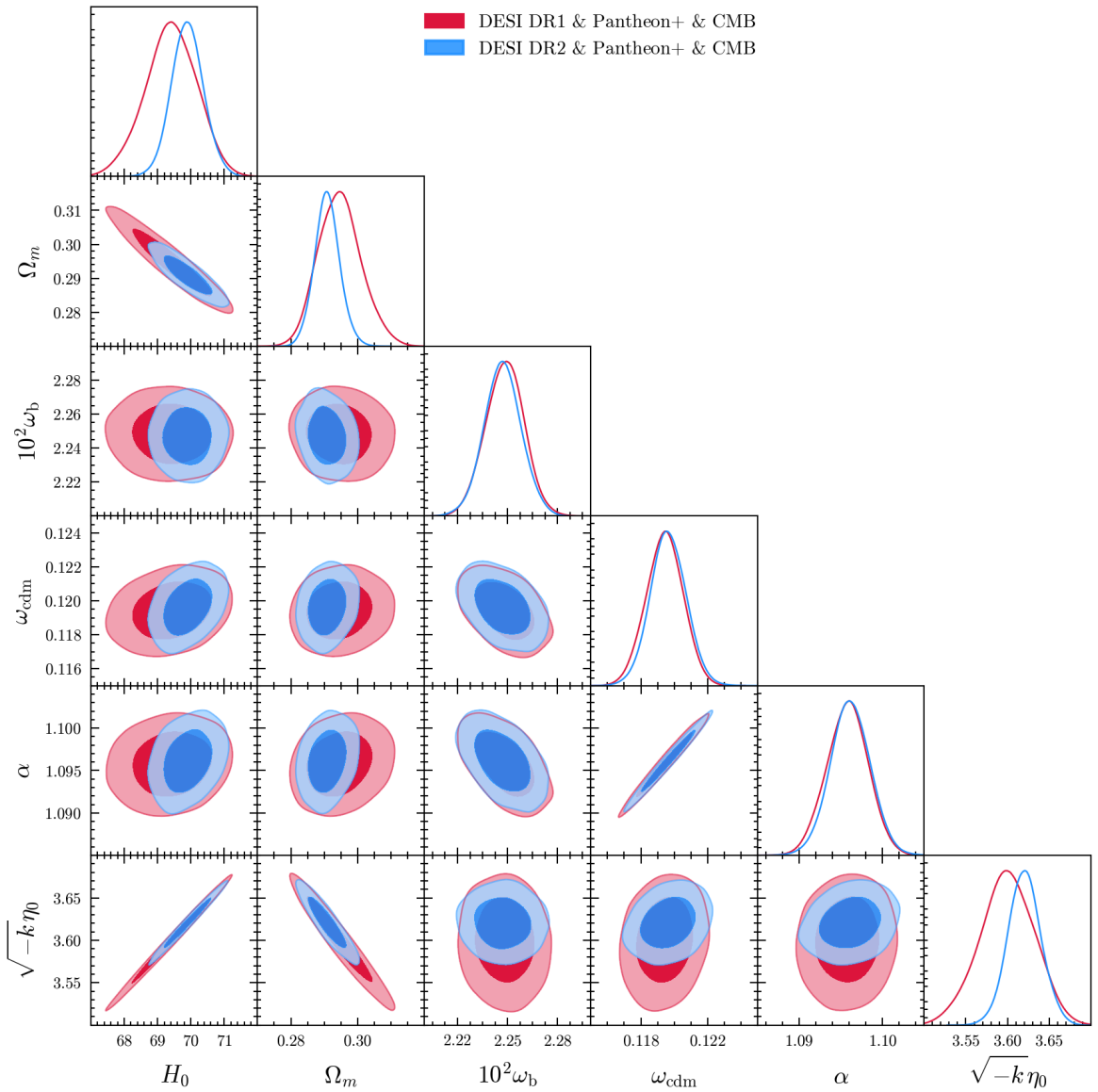


Figure 10. Similar to Fig. 2 but comparing the results using either DESI DR1 or DR2, combined with the Pantheon+ sample and the CMB data from P-ACT. The constraining power in the curvature scale parameter, $\sqrt{-k}\eta_0$, is improved by 60% when moving from DESI DR1 to DESI DR2, including also SNe Ia and CMB data.

C CMB Compression and comparison with CamSpec PR4

In this appendix, we compare the constraints obtained using the CamSpec CMB likelihood, based on the Planck PR4 maps, with those obtained from the Planck and ACT (P-ACT) combination [75, 76]. These results are shown in Fig. 11. The compressed CMB information from the Planck (PR4) chains can be found in Appendix A of Ref. [74]. Here, we provide the equivalent from the P-ACT chains [75]. The data vector and covariance matrix are given by

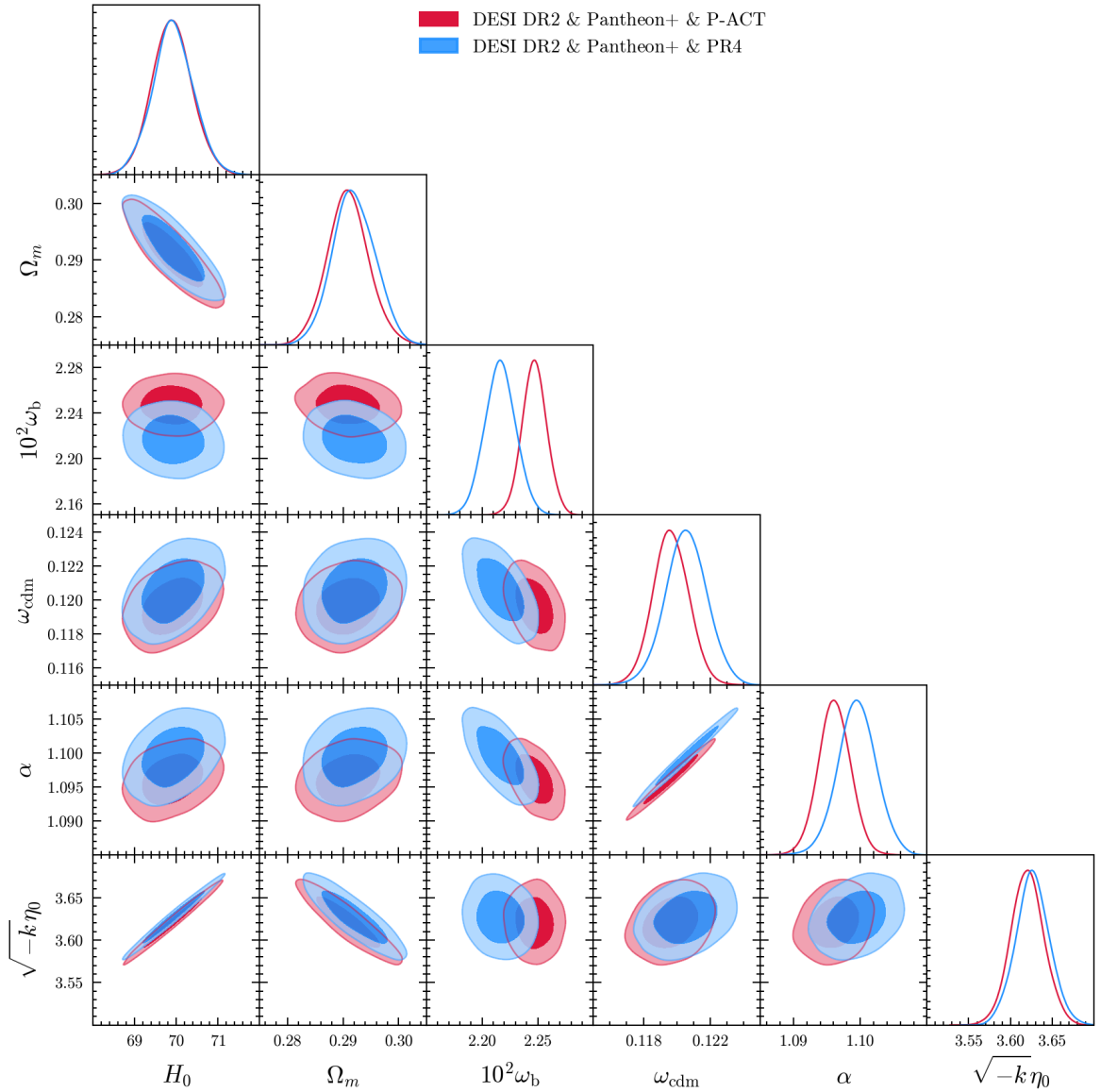


Figure 11. Comparison of the constraints obtained using the compressed CMB measurements of $(\theta_s, \omega_b, \omega_{bc})$ extracted from either Planck (CamSpec) PR4, or the Planck PR3+ACT (P-ACT) combination.

$$\vec{\mathcal{D}} = \begin{pmatrix} 100 \theta_s \\ \omega_b \\ \omega_{bc} \end{pmatrix} = \begin{pmatrix} 1.04165 \\ 0.0225046 \\ 0.141640 \end{pmatrix}, \quad (C.1)$$

$$\Sigma = \begin{pmatrix} 6.64717 \times 10^{-8} & 2.71701 \times 10^{-9} & -3.92400 \times 10^{-8} \\ 2.71701 \times 10^{-9} & 1.20267 \times 10^{-8} & -3.49601 \times 10^{-8} \\ -3.92400 \times 10^{-8} & -3.49601 \times 10^{-8} & 1.11695 \times 10^{-6} \end{pmatrix}, \quad (C.2)$$

from which we construct the likelihood $-2 \ln \mathcal{L} = \chi^2$ in the usual way,

$$\chi^2 = \vec{r}^T \cdot \Sigma^{-1} \cdot \vec{r} \quad (C.3)$$

where \vec{r} is the residual vector between the theoretical predictions and the data vector \vec{D} .

D Author Affiliations

^aCEICO, Institute of Physics of the Czech Academy of Sciences, Na Slovance 1999/2, 182 21, Prague, Czech Republic.

^bInstituto de Física Teórica (IFT) UAM/CSIC, Universidad Autónoma de Madrid, Cantoblanco, E-28049, Madrid, Spain

^cCentro de Investigación Avanzada en Física Fundamental (CIAFF), Facultad de Ciencias, Universidad Autónoma de Madrid, ES-28049 Madrid, Spain

^dKorea Astronomy and Space Science Institute, 776, Daedeokdae-ro, Yuseong-gu, Daejeon 34055, Republic of Korea

^eUniversity of Science and Technology, 217 Gajeong-ro, Yuseong-gu, Daejeon 34113, Republic of Korea

^fLawrence Berkeley National Laboratory, 1 Cyclotron Road, Berkeley, CA 94720, USA

^gDepartment of Physics, Boston University, 590 Commonwealth Avenue, Boston, MA 02215 USA

^hDipartimento di Fisica “Aldo Pontremoli”, Università degli Studi di Milano, Via Celoria 16, I-20133 Milano, Italy

ⁱINAF-Osservatorio Astronomico di Brera, Via Brera 28, 20122 Milano, Italy

^jDepartment of Physics & Astronomy, University College London, Gower Street, London, WC1E 6BT, UK

^kInstituto de Física, Universidad Nacional Autónoma de México, Circuito de la Investigación Científica, Ciudad Universitaria, Cd. de México C. P. 04510, México

^lDepartamento de Física, Universidad de los Andes, Cra. 1 No. 18A-10, Edificio Ip, CP 111711, Bogotá, Colombia

^mObservatorio Astronómico, Universidad de los Andes, Cra. 1 No. 18A-10, Edificio H, CP 111711 Bogotá, Colombia

ⁿInstitut d’Estudis Espacials de Catalunya (IEEC), c/ Esteve Terradas 1, Edifici RDIT, Campus PMT-UPC, 08860 Castelldefels, Spain

^oInstitute of Cosmology and Gravitation, University of Portsmouth, Dennis Sciama Building, Portsmouth, PO1 3FX, UK

^pInstitute of Space Sciences, ICE-CSIC, Campus UAB, Carrer de Can Magrans s/n, 08913 Bellaterra, Barcelona, Spain

^qUniversity of Virginia, Department of Astronomy, Charlottesville, VA 22904, USA

^rFermi National Accelerator Laboratory, PO Box 500, Batavia, IL 60510, USA

^sCenter for Cosmology and AstroParticle Physics, The Ohio State University, 191 West Woodruff Avenue, Columbus, OH 43210, USA

^tDepartment of Physics, The Ohio State University, 191 West Woodruff Avenue, Columbus, OH 43210, USA

^uThe Ohio State University, Columbus, 43210 OH, USA

^vSchool of Mathematics and Physics, University of Queensland, Brisbane, QLD 4072, Australia

^wDepartment of Physics, The University of Texas at Dallas, 800 W. Campbell Rd., Richardson, TX 75080, USA

^xNSF NOIRLab, 950 N. Cherry Ave., Tucson, AZ 85719, USA

^yDepartment of Physics, Southern Methodist University, 3215 Daniel Avenue, Dallas, TX 75275, USA

^zDepartament de Física, Serra Húnter, Universitat Autònoma de Barcelona, 08193 Bellaterra (Barcelona), Spain

^{aa}Institut de Física d'Altes Energies (IFAE), The Barcelona Institute of Science and Technology, Edifici Cn, Campus UAB, 08193, Bellaterra (Barcelona), Spain

^{ab}Institució Catalana de Recerca i Estudis Avançats, Passeig de Lluís Companys, 23, 08010 Barcelona, Spain

^{ac}Instituto de Astrofísica de Andalucía (CSIC), Glorieta de la Astronomía, s/n, E-18008 Granada, Spain

^{ad}Departament de Física, EEBE, Universitat Politècnica de Catalunya, c/Eduard Maristany 10, 08930 Barcelona, Spain

^{ae}CIEMAT, Avenida Complutense 40, E-28040 Madrid, Spain

^{af}Department of Physics, University of Michigan, 450 Church Street, Ann Arbor, MI 48109, USA

^{ag}University of Michigan, 500 S. State Street, Ann Arbor, MI 48109, USA

^{ah}National Astronomical Observatories, Chinese Academy of Sciences, A20 Datun Road, Chaoyang District, Beijing, 100101, P. R. China

References

- [1] V. Sahni and A.A. Starobinsky, *The Case for a positive cosmological Lambda term*, *Int. J. Mod. Phys. D* **9** (2000) 373 [[astro-ph/9904398](#)].
- [2] SUPERNOVA SEARCH TEAM collaboration, *Observational evidence from supernovae for an accelerating universe and a cosmological constant*, *Astron. J.* **116** (1998) 1009 [[astro-ph/9805201](#)].
- [3] SUPERNOVA COSMOLOGY PROJECT collaboration, *Measurements of Ω and Λ from 42 High Redshift Supernovae*, *Astrophys. J.* **517** (1999) 565 [[astro-ph/9812133](#)].
- [4] N. Aghanim, Y. Akrami, F. Arroja, M. Ashdown, J. Aumont, C. Baccigalupi et al., *Planck2018 results: I. overview and the cosmological legacy of planck*, *Astronomy & Astrophysics* **641** (2020) A1.
- [5] S. Alam, M. Aubert, S. Avila, C. Balland, J.E. Bautista, M.A. Bershady et al., *Completed sdss-iv extended baryon oscillation spectroscopic survey: Cosmological implications from two decades of spectroscopic surveys at the apache point observatory*, *Physical Review D* **103** (2021) .
- [6] C. Zhao, A. Variu, M. He, D. Forero-Sánchez, A. Tamone, C.-H. Chuang et al., *The completed sdss-iv extended baryon oscillation spectroscopic survey: cosmological implications from multitracer bao analysis with galaxies and voids*, *Monthly Notices of the Royal Astronomical Society* **511** (2022) 5492–5524.
- [7] S. Weinberg, *The Cosmological Constant Problem*, *Rev. Mod. Phys.* **61** (1989) 1.
- [8] S.M. Carroll, *The Cosmological constant*, *Living Rev. Rel.* **4** (2001) 1 [[astro-ph/0004075](#)].
- [9] P. Bull et al., *Beyond Λ CDM: Problems, solutions, and the road ahead*, *Phys. Dark Univ.* **12** (2016) 56 [[1512.05356](#)].
- [10] J.S. Bullock and M. Boylan-Kolchin, *Small-Scale Challenges to the Λ CDM Paradigm*, *Ann. Rev. Astron. Astrophys.* **55** (2017) 343 [[1707.04256](#)].
- [11] L. Perivolaropoulos and F. Skara, *Challenges for Λ CDM: An update*, *New Astron. Rev.* **95** (2022) 101659 [[2105.05208](#)].

[12] E. Abdalla et al., *Cosmology intertwined: A review of the particle physics, astrophysics, and cosmology associated with the cosmological tensions and anomalies*, *JHEAp* **34** (2022) 49 [[2203.06142](#)].

[13] R. Calderón, A. Shafieloo, D.K. Hazra and W. Sohn, *On the consistency of Λ CDM with CMB measurements in light of the latest Planck, ACT and SPT data*, *JCAP* **08** (2023) 059 [[2302.14300](#)].

[14] A.G. Riess et al., *A Comprehensive Measurement of the Local Value of the Hubble Constant with 1 km/s/Mpc Uncertainty from the Hubble Space Telescope and the SH0ES Team*, [2112.04510](#).

[15] E. Di Valentino, O. Mena, S. Pan, L. Visinelli, W. Yang, A. Melchiorri et al., *In the realm of the Hubble tension—a review of solutions*, *Class. Quant. Grav.* **38** (2021) 153001 [[2103.01183](#)].

[16] N. Schöneberg, G. Franco Abellán, A. Pérez Sánchez, S.J. Witte, V. Poulin and J. Lesgourgues, *The H_0 Olympics: A fair ranking of proposed models*, *Phys. Rept.* **984** (2022) 1 [[2107.10291](#)].

[17] A.H. Wright et al., *KiDS-Legacy: Cosmological constraints from cosmic shear with the complete Kilo-Degree Survey*, [2503.19441](#).

[18] HSC collaboration, *Cosmology from cosmic shear power spectra with Subaru Hyper Suprime-Cam first-year data*, *Publ. Astron. Soc. Jap.* **71** (2019) 43 [[1809.09148](#)].

[19] KiDS collaboration, *KiDS-1000 Cosmology: Cosmic shear constraints and comparison between two point statistics*, *Astron. Astrophys.* **645** (2021) A104 [[2007.15633](#)].

[20] DES collaboration, *Dark Energy Survey Year 3 results: Cosmological constraints from galaxy clustering and weak lensing*, *Phys. Rev. D* **105** (2022) 023520 [[2105.13549](#)].

[21] E. Di Valentino et al., *Cosmology Intertwined III: $f\sigma_8$ and S_8* , *Astropart. Phys.* **131** (2021) 102604 [[2008.11285](#)].

[22] DESI collaboration, *DESI 2024 VI: Cosmological Constraints from the Measurements of Baryon Acoustic Oscillations*, [2404.03002](#).

[23] DESI collaboration, *Extended Dark Energy analysis using DESI DR2 BAO measurements*, [2503.14743](#).

[24] DESI collaboration, *DESI 2024: reconstructing dark energy using crossing statistics with DESI DR1 BAO data*, *JCAP* **10** (2024) 048 [[2405.04216](#)].

[25] DESI Collaboration, A.G. Adame, J. Aguilar, S. Ahlen, S. Alam, D.M. Alexander et al., *DESI 2024 VII: Cosmological Constraints from the Full-Shape Modeling of Clustering Measurements*, *arXiv e-prints* (2024) arXiv:2411.12022 [[2411.12022](#)].

[26] DESI collaboration, *DESI 2024: Constraints on physics-focused aspects of dark energy using DESI DR1 BAO data*, *Phys. Rev. D* **111** (2025) 023532 [[2405.13588](#)].

[27] M. Ishak et al., *Modified Gravity Constraints from the Full Shape Modeling of Clustering Measurements from DESI 2024*, [2411.12026](#).

[28] K. Lodha, R. Calderon, W.L. Matthewson, A. Shafieloo, M. Ishak, J. Pan et al., *Extended Dark Energy analysis using DESI DR2 BAO measurements*, *arXiv e-prints* (2025) arXiv:2503.14743 [[2503.14743](#)].

[29] DESI collaboration, *Dynamical Dark Energy in light of the DESI DR2 Baryonic Acoustic Oscillations Measurements*, [2504.06118](#).

[30] W. Elbers, C.S. Frenk, A. Jenkins, B. Li and S. Pascoli, *Negative neutrino masses as a mirage of dark energy*, *Phys. Rev. D* **111** (2025) 063534 [[2407.10965](#)].

[31] DESI collaboration, *Constraints on Neutrino Physics from DESI DR2 BAO and DR1 Full Shape*, [2503.14744](#).

[32] X. Chen and A. Loeb, *Evolving Dark Energy or Evolving Dark Matter?*, [2505.02645](#).

[33] G.P. Lynch, L. Knox and J. Chluba, *DESI observations and the Hubble tension in light of modified recombination*, *Phys. Rev. D* **110** (2024) 083538 [[2406.10202](#)].

[34] DESI collaboration, *Positive neutrino masses with DESI DR2 via matter conversion to dark energy*, [2504.20338](#).

[35] E. Chaussidon et al., *Early time solution as an alternative to the late time evolving dark energy with DESI DR2 BAO*, [2503.24343](#).

[36] S.-F. Chen and M. Zaldarriaga, *It's All Ok: Curvature in Light of BAO from DESI DR2*, [2505.00659](#).

[37] S.H. Mirpoorian, K. Jedamzik and L. Pogosian, *Is Dynamical Dark Energy Necessary? DESI BAO and Modified Recombination*, [2504.15274](#).

[38] N. Sailer, G.S. Farren, S. Ferraro and M. White, *Disputable: the high cost of a low optical depth*, [2504.16932](#).

[39] A. Shafieloo, U. Alam, V. Sahni and A.A. Starobinsky, *Smoothing Supernova Data to Reconstruct the Expansion History of the Universe and its Age*, *Mon. Not. Roy. Astron. Soc.* **366** (2006) 1081 [[astro-ph/0505329](#)].

[40] T. Holsclaw, U. Alam, B. Sansó, H. Lee, K. Heitmann, S. Habib et al., *Nonparametric reconstruction of the dark energy equation of state*, *Phys. Rev. D* **82** (2010) 103502 [[1009.5443](#)].

[41] A. Shafieloo, A.G. Kim and E.V. Linder, *Gaussian process cosmography*, *Phys. Rev. D* **85** (2012) 123530 [[1204.2272](#)].

[42] S. Nesseris and J. García-Bellido, *A new perspective on dark energy modeling via genetic algorithms*, *Journal of Cosmology and Astroparticle Physics* **2012** (2012) 033–033.

[43] R. Calderón, B. L’Huillier, D. Polarski, A. Shafieloo and A.A. Starobinsky, *Joint reconstructions of growth and expansion histories from stage-IV surveys with minimal assumptions: Dark energy beyond Λ* , *Phys. Rev. D* **106** (2022) 083513 [[2206.13820](#)].

[44] R. Calderón, B. L’Huillier, D. Polarski, A. Shafieloo and A.A. Starobinsky, *Joint reconstructions of growth and expansion histories from stage-IV surveys with minimal assumptions. II. Modified gravity and massive neutrinos*, *Phys. Rev. D* **108** (2023) 023504 [[2301.00640](#)].

[45] M. Chevallier and D. Polarski, *Accelerating universes with scaling dark matter*, *Int. J. Mod. Phys. D* **10** (2001) 213 [[gr-qc/0009008](#)].

[46] E.V. Linder, *Exploring the expansion history of the universe*, *Phys. Rev. Lett.* **90** (2003) 091301 [[astro-ph/0208512](#)].

[47] R.R. Caldwell and E.V. Linder, *The Limits of quintessence*, *Phys. Rev. Lett.* **95** (2005) 141301 [[astro-ph/0505494](#)].

[48] R. de Putter and E.V. Linder, *Calibrating Dark Energy*, *JCAP* **10** (2008) 042 [[0808.0189](#)].

[49] J. García-Bellido and L. Espinosa-Portalés, *Cosmic acceleration from first principles*, *Phys. Dark Univ.* **34** (2021) 100892 [[2106.16014](#)].

[50] L. Espinosa-Portalés and J. García-Bellido, *Covariant formulation of non-equilibrium thermodynamics in General Relativity*, *Phys. Dark Univ.* **34** (2021) 100893 [[2106.16012](#)].

[51] J. García-Bellido, *Cosmic entropic acceleration from supermassive black hole growth*, *Phys. Dark Univ.* **44** (2024) 101491 [[2306.10593](#)].

[52] DES collaboration, *The Dark Energy Survey: Cosmology Results with ~ 1500 New High-redshift Type Ia Supernovae Using the Full 5 yr Data Set*, *Astrophys. J. Lett.* **973** (2024) L14 [[2401.02929](#)].

[53] DESI collaboration, *DESI 2024 V: Full-Shape galaxy clustering from galaxies and quasars*, *JCAP* **09** (2025) 008 [[2411.12021](#)].

[54] R. Arjona, L. Espinosa-Portales, J. García-Bellido and S. Nesseris, *A GREAT model comparison against the cosmological constant*, *Phys. Dark Univ.* **36** (2022) 101029 [[2111.13083](#)].

[55] J. García-Bellido, *Dark Energy predictions from GREA: Background and linear perturbation theory*, *Phys. Dark Univ.* **45** (2024) 101533 [[2405.02895](#)].

[56] DESI Collaboration, A.G. Adame, J. Aguilar, S. Ahlen, S. Alam, D.M. Alexander et al., *DESI 2024 VI: cosmological constraints from the measurements of baryon acoustic oscillations*, *J. Cosmology Astropart. Phys.* **2025** (2025) 021 [[2404.03002](#)].

[57] DESI Collaboration, A.G. Adame, J. Aguilar, S. Ahlen, S. Alam, D.M. Alexander et al., *DESI 2024 III: baryon acoustic oscillations from galaxies and quasars*, *J. Cosmology Astropart. Phys.* **2025** (2025) 012 [[2404.03000](#)].

[58] M. Levi, C. Bebek, T. Beers, R. Blum, R. Cahn, D. Eisenstein et al., *The DESI Experiment, a whitepaper for Snowmass 2013*, *arXiv e-prints* (2013) arXiv:1308.0847 [[1308.0847](#)].

[59] DESI Collaboration, A. Aghamousa, J. Aguilar, S. Ahlen, S. Alam, L.E. Allen et al., *The DESI Experiment Part II: Instrument Design*, *arXiv e-prints* (2016) arXiv:1611.00037 [[1611.00037](#)].

[60] DESI Collaboration, B. Abareshi, J. Aguilar, S. Ahlen, S. Alam, D.M. Alexander et al., *Overview of the Instrumentation for the Dark Energy Spectroscopic Instrument*, *AJ* **164** (2022) 207 [[2205.10939](#)].

[61] J.H. Silber, P. Fagrelius, K. Fanning, M. Schubnell, J.N. Aguilar, S. Ahlen et al., *The Robotic Multiobject Focal Plane System of the Dark Energy Spectroscopic Instrument (DESI)*, *AJ* **165** (2023) 9 [[2205.09014](#)].

[62] T.N. Miller, P. Doel, G. Gutierrez, R. Besuner, D. Brooks, G. Gallo et al., *The Optical Corrector for the Dark Energy Spectroscopic Instrument*, *AJ* **168** (2024) 95 [[2306.06310](#)].

[63] J. Guy, S. Bailey, A. Kremin, S. Alam, D.M. Alexander, C. Allende Prieto et al., *The Spectroscopic Data Processing Pipeline for the Dark Energy Spectroscopic Instrument*, *AJ* **165** (2023) 144 [[2209.14482](#)].

[64] E.F. Schlafly, D. Kirkby, D.J. Schlegel, A.D. Myers, A. Raichoor, K. Dawson et al., *Survey Operations for the Dark Energy Spectroscopic Instrument*, *AJ* **166** (2023) 259 [[2306.06309](#)].

[65] C. Poppett, L. Tyas, J. Aguilar, C. Bebek, D. Bramall, T. Claybaugh et al., *Overview of the Fiber System for the Dark Energy Spectroscopic Instrument*, *AJ* **168** (2024) 245.

[66] DESI Collaboration, A. Aghamousa, J. Aguilar, S. Ahlen, S. Alam, L.E. Allen et al., *The DESI Experiment Part I: Science, Targeting, and Survey Design*, *arXiv e-prints* (2016) arXiv:1611.00036 [[1611.00036](#)].

[67] DESI Collaboration, A.G. Adame, J. Aguilar, S. Ahlen, S. Alam, G. Aldering et al., *Validation of the Scientific Program for the Dark Energy Spectroscopic Instrument*, *AJ* **167** (2024) 62 [[2306.06307](#)].

[68] DESI Collaboration, A.G. Adame, J. Aguilar, S. Ahlen, S. Alam, G. Aldering et al., *The Early Data Release of the Dark Energy Spectroscopic Instrument*, *AJ* **168** (2024) 58 [[2306.06308](#)].

[69] DESI Collaboration, A.G. Adame, J. Aguilar, S. Ahlen, S. Alam, D.M. Alexander et al.,

DESI 2024 IV: Baryon Acoustic Oscillations from the Lyman alpha forest, *J. Cosmology Astropart. Phys.* **2025** (2025) 124 [[2404.03001](#)].

[70] DESI Collaboration, M. Abdul-Karim, J. Aguilar, S. Ahlen, S. Alam, L. Allen et al., *DESI DR2 Results II: Measurements of Baryon Acoustic Oscillations and Cosmological Constraints*, *arXiv e-prints* (2025) arXiv:2503.14738 [[2503.14738](#)].

[71] A. Aizpuru, R. Arjona and S. Nesseris, *Machine learning improved fits of the sound horizon at the baryon drag epoch*, *Phys. Rev. D* **104** (2021) 043521 [[2106.00428](#)].

[72] D. Brout et al., *The Pantheon+ Analysis: Cosmological Constraints*, *Astrophys. J.* **938** (2022) 110 [[2202.04077](#)].

[73] D. Rubin et al., *Union Through UNITY: Cosmology with 2,000 SNe Using a Unified Bayesian Framework*, [2311.12098](#).

[74] DESI collaboration, *DESI DR2 Results II: Measurements of Baryon Acoustic Oscillations and Cosmological Constraints*, [2503.14738](#).

[75] ACT collaboration, *The Atacama Cosmology Telescope: DR6 Power Spectra, Likelihoods and Λ CDM Parameters*, [2503.14452](#).

[76] ACT collaboration, *The Atacama Cosmology Telescope: DR6 Constraints on Extended Cosmological Models*, [2503.14454](#).

[77] J. Carron, M. Mirmelstein and A. Lewis, *CMB lensing from Planck PR4 maps*, *JCAP* **09** (2022) 039 [[2206.07773](#)].

[78] ACT collaboration, *The Atacama Cosmology Telescope: DR6 Gravitational Lensing Map and Cosmological Parameters*, *Astrophys. J.* **962** (2024) 113 [[2304.05203](#)].

[79] ACT collaboration, *The Atacama Cosmology Telescope: A Measurement of the DR6 CMB Lensing Power Spectrum and Its Implications for Structure Growth*, *Astrophys. J.* **962** (2024) 112 [[2304.05202](#)].

[80] N. Schöneberg, *The 2024 BBN baryon abundance update*, *JCAP* **06** (2024) 006 [[2401.15054](#)].

[81] A. Lewis and S. Bridle, *Cosmological parameters from CMB and other data: A Monte Carlo approach*, *Phys. Rev. D* **66** (2002) 103511 [[astro-ph/0205436](#)].

[82] A. Lewis, *Efficient sampling of fast and slow cosmological parameters*, *Phys. Rev. D* **87** (2013) 103529 [[1304.4473](#)].

[83] J. Torrado and A. Lewis, *Cobaya: Code for Bayesian Analysis of hierarchical physical models*, *J. Cosmology Astropart. Phys.* **05** (2021) 057 [[2005.05290](#)].

[84] A. Gelman and D.B. Rubin, *Inference from Iterative Simulation Using Multiple Sequences*, *Statistical Science* **7** (1992) 457.

[85] A. Lewis, *GetDist: a Python package for analysing Monte Carlo samples*, 2019.

[86] J. Pan, D. Huterer, F. Andrade-Oliveira and C. Avestruz, *Compressed baryon acoustic oscillation analysis is robust to modified-gravity models*, *JCAP* **06** (2024) 051 [[2312.05177](#)].

[87] W.J. Handley, M.P. Hobson and A.N. Lasenby, *PolyChord: nested sampling for cosmology*, *Mon. Not. Roy. Astron. Soc.* **450** (2015) L61 [[1502.01856](#)].

[88] W.J. Handley, M.P. Hobson and A.N. Lasenby, *polychord: next-generation nested sampling*, *Monthly Notices of the Royal Astronomical Society* **453** (2015) 4385–4399.

[89] S. Nesseris and J. García-Bellido, *Is the jeffreys' scale a reliable tool for bayesian model comparison in cosmology?*, *Journal of Cosmology and Astroparticle Physics* **2013** (2013) 036.

[90] H. Koo, R.E. Keeley, A. Shafieloo and B. L’Huillier, *Bayesian vs frequentist: comparing bayesian model selection with a frequentist approach using the iterative smoothing method*, *Journal of Cosmology and Astroparticle Physics* **2022** (2022) 047.

[91] R.E. Keeley and A. Shafieloo, *On the distribution of Bayesian evidence*, *Monthly Notices of the Royal Astronomical Society* **515** (2022) 293 [<https://academic.oup.com/mnras/article-pdf/515/1/293/44885825/stac1851.pdf>].

[92] V. Poulin, T.L. Smith, R. Calderón and T. Simon, *Implications of the cosmic calibration tension beyond H_0 and the synergy between early- and late-time new physics*, *Phys. Rev. D* **111** (2025) 083552 [[2407.18292](#)].

[93] D. Pedrotti, J.-Q. Jiang, L.A. Escamilla, S.S. da Costa and S. Vagnozzi, *Multidimensionality of the Hubble tension: The roles of Ωm and ω_c* , *Phys. Rev. D* **111** (2025) 023506 [[2408.04530](#)].

[94] M. Chu and L. Knox, *Testing cosmological models and understanding cosmological parameter determinations with metaparameters*, *Astrophys. J.* **620** (2005) 1 [[astro-ph/0407198](#)].

[95] P. Motloch, *Testing consistency of $\Omega b h^2$ in the Planck data*, *Phys. Rev. D* **101** (2020) 123509 [[2004.11351](#)].

[96] I. Wasserman, *On the degeneracy inherent in observational determination of the dark energy equation of state*, *Phys. Rev. D* **66** (2002) 123511 [[astro-ph/0203137](#)].

[97] M. Kunz, *Degeneracy between the dark components resulting from the fact that gravity only measures the total energy-momentum tensor*, *Phys. Rev. D* **80** (2009) 123001.

[98] A. Shafieloo and E.V. Linder, *Cosmographic Degeneracy*, *Phys. Rev. D* **84** (2011) 063519 [[1107.1033](#)].

[99] R. von Marttens, L. Lombriser, M. Kunz, V. Marra, L. Casarini and J. Alcaniz, *Dark degeneracy i: Dynamical or interacting dark energy?*, *Physics of the Dark Universe* **28** (2020) 100490.

[100] R.E. Keeley and A. Shafieloo, *Ruling out new physics at low redshift as a solution to the H_0 tension*, *Phys. Rev. Lett.* **131** (2023) 111002.

[101] H. Dembinski, P. Ongmongkolkul and et al., scikit-hep/iminuit, *Zenodo* (2020) .

[102] DESI Collaboration, A.G. Adame, J. Aguilar, S. Ahlen, S. Alam, D.M. Alexander et al., *DESI 2024 II: Sample Definitions, Characteristics, and Two-point Clustering Statistics*, *arXiv e-prints* (2024) [arXiv:2411.12020](#) [[2411.12020](#)].

[103] Y.-S. Song and W.J. Percival, *Reconstructing the history of structure formation using Redshift Distortions*, *JCAP* **10** (2009) 004 [[0807.0810](#)].

[104] P.J.E. Peebles, *The Peculiar Velocity Field in the Local Supercluster*, *ApJ* **205** (1976) 318.

[105] O. Lahav, P.B. Lilje, J.R. Primack and M.J. Rees, *Dynamical effects of the cosmological constant.*, *MNRAS* **251** (1991) 128.

[106] L.-M. Wang and P.J. Steinhardt, *Cluster abundance constraints on quintessence models*, *Astrophys. J.* **508** (1998) 483 [[astro-ph/9804015](#)].

[107] E.V. Linder, *Cosmic growth history and expansion history*, *Phys. Rev. D* **72** (2005) 043529 [[astro-ph/0507263](#)].

[108] D. Polarski and R. Gannouji, *On the growth of linear perturbations*, *Phys. Lett. B* **660** (2008) 439 [[0710.1510](#)].

[109] D. Polarski, A.A. Starobinsky and H. Giacomini, *When is the growth index constant?*, *JCAP* **12** (2016) 037 [[1610.00363](#)].

[110] R. Calderon, D. Felbacq, R. Gannouji, D. Polarski and A.A. Starobinsky, *Global properties of the growth index of matter inhomogeneities in the universe*, *Phys. Rev. D* **100** (2019) 083503 [[1908.00117](#)].

- [111] R. Calderon, D. Felbacq, R. Gannouji, D. Polarski and A.A. Starobinsky, *Global properties of the growth index: mathematical aspects and physical relevance*, *Phys. Rev. D* **101** (2020) 103501 [[1912.06958](#)].
- [112] L. Amendola et al., *Cosmology and fundamental physics with the Euclid satellite*, *Living Rev. Rel.* **21** (2018) 2 [[1606.00180](#)].